# Product Distributions from Molecular Mechanics−Valence Bond Dynamics: Modeling Photochemical [4 + 4] Cycloadditions

Mercè Deumal,[†] Michael J. Bearpark,[‡] Barry R. Smith,[‡] Massimo Olivucci,*[,§] Fernando Bernardi,[§] and Michael A. Robb*[,‡]

*Departament de Química Física, Universitat de Barcelona, Martí i Franquès 1, 08028 Barcelona, Spain, Department of Chemistry, King's College London, Strand, London WC2R 2LS, U.K., and Dipartimento di Chimica 'G. Ciamician' dell' Università di Bologna, Via Selmi 2, 40126 Bologna, Italy*

*Received November 18, 1997*

The purpose of this paper is to study the model [4 + 4] photocycloaddition of butadiene + butadiene by using direct dynamics calculations—with no geometric constraints—to describe motion along excited-state reaction paths and subsequent decay to the ground state. We use the molecular mechanics−valence bond (MMVB) potential, which is calibrated against previous CASSCF calculations for this system (Bearpark, M. J.; Deumal, M.; Robb, M. A.; Vreven, T.; Yamamoto, N.; Olivucci, M.; Bernardi, F. *J. Am. Chem. Soc.* **1997**, *119*, 709−718). Our dynamics calculations show that efficient nonradiative decay of butadiene + butadiene in the presence of two different $S_1/S_0$ conical intersections can account for the formation of many products. The major product predicted by MMVB is consistent with the limited experimental data available.

## 1. Introduction

In a molecular dynamics simulation, one obtains geometries and energies as a function of time. For a suitable choice of initial conditions, these data can be used to generate a product distribution that can be compared directly with experimental product yields. However, the cost of accurate quantum (wave packet) dynamics computations[1] for many nuclear degrees of freedom is prohibitive, so there is a need to be pragmatic and adopt an approach that is sufficiently accurate yet computationally feasible. In photochemistry the problem is more severe because the dynamics must be propagated on more than one potential energy surface, including the effect of the nonadiabatic transition.

We have developed[2,3] an approach for combining quantum chemistry with dynamics where the gradients that are used to drive the dynamics simulation are evaluated "on the fly" using a hybrid molecular mechanics valence bond (MMVB) method. Our purpose in this paper is to show how such a method can be used to model the photoproduct distribution for a photochemical reaction with two competing excited-state branches—the [4 + 4] photocycloaddition of butadiene + butadiene[4,5]—which is a model for diene + aromatic photoadditions in general.[6−12] The major product predicted for butadiene + butadiene by MMVB dynamics is consistent with the limited experimental data available.[5c]

On the excited-state potential energy surface of the butadiene + butadiene model system (Scheme 1) we have characterized[4] a true pericyclic minimum **A** and two independent reaction channels leading via transition structures **B** and **D** to conical intersections **C** and **E**. Both conical intersections are tetraradicaloids: fully efficient decay to the ground state in the vicinity of either **C** or **E** can lead to three primary photoproducts, because there are three ways in which the almost-unpaired electrons can recouple.[13] Any biradical intermediates thus formed (far right, Scheme 1) will react further to form secondary

[†] Universitat de Barcelona.
[‡] King's College London.
[§] Università di Bologna.

(1) For a recent review see Domcke, W.; Stock, G. *Adv. Chem. Phys.* **1997**, *100* 1−169.
(2) Smith, B. R.; Bearpark, M. J.; Robb, M. A.; Bernardi, F.; Olivucci, M. *Chem. Phys. Lett.* **1995**, *242*, 27−32.
(3) (a) Bearpark, M. J.; Bernardi, F.; Clifford, S.; Olivucci, M.; Robb, M. A.; Smith, B. R.; Vreven, T. *J. Am. Chem. Soc.* **1996**, *118*, 169−175. (b) Bearpark, M. J.; Bernardi, F.; Olivucci, M.; Robb, M. A.; Smith, B. R. *J. Am. Chem. Soc.* **1996**, *118*, 5254−5260. (c) Clifford, S.; Bearpark, M. J.; Bernardi, F.; Olivucci, M.; Robb, M. A.; Smith, B. R. *J. Am. Chem. Soc.* **1996**, *118*, 7353−7360.
(4) Bearpark, M. J.; Deumal, M.; Robb, M. A.; Vreven, T.; Yamamoto, N.; Olivucci, M.; Bernardi, F. *J. Am. Chem. Soc.* **1997**, *119*, 709−718.
(5) (a) Srinivasen, R. *J. Am. Chem. Soc.* **1960**, *82*, 5063−5066. (b) Haller, I.; Srinivasen, R. *J. Chem. Phys.* **1964**, *40*, 1992−1997. (c) Srinivasen, R.; Sonntag, F. I. *J. Am. Chem. Soc.* **1965**, *87*, 3778−3779.
(6) Stephenson, L. M.; Whitten, D. G.; Vesley, G. F.; Hammond, G. S. *J. Am. Chem. Soc.* **1966**, *88*, 3665−3666, 3893.
(7) For reviews of [4 + 4] cycloadditions, see: (a) Bouas-Laurent, H.; Desvergne, J.-P. In *Photochromism: Molecules and Systems*; Dürr, H., Bouas-Laurent, H., Eds.; Elsevier: Amsterdam, 1990; Chapter 14**.** (b) Dilling, W. L. *Chem. Rev.* **1969**, *69*, 845−877. (c) Cowan, D. O.; Drisko, R. L. *Elements of Organic Photochemistry*; Plenum Press: New York, 1976; pp 388−480. (d) Turro, N. J. *Modern Molecular Photochemistry*; Benjamin/Cummings: Menlo Park, CA, 1978. (e) Stevens, B. *Adv. Photochem.* **1971**, *8*, 161−226. (f) McCullough, J. J. *Chem. Rev.* **1987**, *87*, 811−860.
(8) (a) Koltzenburg, G.; Kraft, H. *Angew. Chem., Int. Ed. Engl.* **1965**, *4*, 981−982. (b) Yang, N. C.; Libman, J. *Tetrahedron Lett.* **1973**, 1409−1412.
(9) (a) Kraft, H.; Koltzenburg, G. *Tetrahedron Lett.* **1967**, 4723−4728. (b) Yang, N. C.; Libman, J.; Savitzky, M. F. *J. Am. Chem. Soc.* **1972**, *94*, 9226−9227. (c) Yang, N. C.; Libman, J. *J. Am. Chem. Soc.* **1972**, *94*, 9228−9229.
(10) (a) Yang, N. C.; Libman, J. *J. Am. Chem. Soc.* **1972**, *94*, 1405−1406. (b) Kaupp, G.; Grüter, H.-W. *Angew. Chem., Int. Ed. Engl.* **1972**, *11*, 313−314. (c) Yang, N. C.; Shold, D. M.; McVey, J. K. *J. Am. Chem. Soc.* **1975**, *97*, 5004−5005. (d) Yang, N. C.; Srinivasachar, K.; Kim, B.; Libman, J. *J. Am. Chem. Soc.* **1975**, *97*, 5006−5008. (e) Yang, N. C.; Shold, D. M.; *J. Chem. Soc. Chem. Commun.* **1978**, 978. (f) Yang, N. C.; Yates, R. L.; Masnovi, J.; Shold, D. M.; Chiang, W. *Pure Appl. Chem.* **1979**, *51*, 173−180.
(11) (a) Saltiel, J.; Townsend, D. E. *J. Am. Chem. Soc.* **1973**, *95*, 6140−6142. (b) Saltiel, J.; Dabestani, R.; Sears, D. F.; McGowan, W. M.; Hilinski, E. F.; *J. Am. Chem. Soc.* **1995**, *117*, 9129−9138.
(12) Chang, S. L. P.; Schuster, D. I. *J. Phys. Chem.* **1987**, *91*, 3644−3649.
(13) (a) Celani, P.; Bernardi, F.; Olivucci, M.; Robb, M. A. *J. Chem. Phys.* **1995**, *102*, 5733−5742. (b) Garavelli, M.; Celani, P.; Fato, M.; Bearpark, M. J.; Smith, B. R.; Olivucci, M.; Robb, M. A. *J. Phys. Chem. A* **1997**, *101*, 2023−2032.

S0022-3263(97)02111-7 CCC: $15.00 
Published on Web 06/23/1998

**Scheme 1**

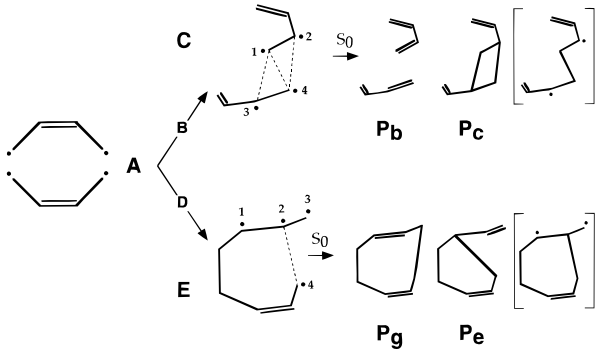


**Scheme 2. $S_0$ Products (Conformation Ignored)**

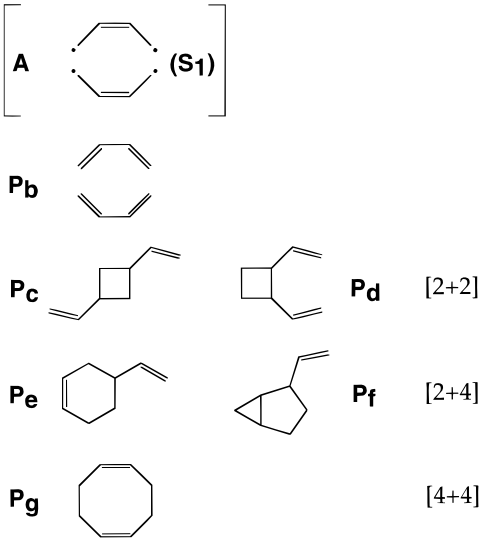


products. (Scheme 2 shows all of the products $\mathbf{P_{b-g}}$ characterized in this study, which include [2 + 2], [2 + 4], and [4 + 4] addition products). The existence of the two $S_1$ reaction paths **ABC** and **ADE** with different barrier heights, together with a complex network of ground-state relaxation paths, suggests that the final distribution of products for photochemical [4 + 4] additions will depend considerably upon the specific reactant structures and experimental conditions.

As well as accounting for the formation of several products, decay funnels such as **C** and **E** can explain two other features of diene + aromatic photoadditions in general,[7] e.g. butadiene + benzene,[8] naphthalene,[9] and anthracene.[10−12] First, dienes have been found to quench the fluorescence of aromatic molecules,[6] implying a rapid and efficient route to $S_0$ such as a surface crossing. Second, there is evidence that these reactions are "concerted":[10a,f] if the dominant ground-state conformer of a diene is trans,[14,15] then a strained trans addition product is formed, suggesting that there is no intermediate at which rearrangement could take place to form the cis product, which is thermodynamically more stable. On the basis of our previous calculations,[4] we make the assumption that both the $S_1$ quenching and photochemical reaction channels involve structures **C** and **E**. After decay in the vicinity of these points, the system will branch toward one of the primary photoproducts, which may (path **ABC**) be the reactants on $S_0$ ($\mathbf{P_b}$). In our simulation, the yield of the different photoproducts is proportional to the number of trajectories leading toward that species.

## 2. Computational Details and Model Validation

MMVB[16] is a hybrid method, which uses the MM2 potential[17] to describe the inert molecular $\sigma$-bonded framework and a Heisenberg Hamiltonian[18] to represent electrons on $sp^2/sp^3$ carbon atoms which are involved in $\pi$-conjugation or new $\sigma$-bond formation. It is a sufficiently inexpensive method of simulating CASSCF calculations for ground and valence excited states[3,16b,19] that many hundreds of trajectories can be calculated on contemporary workstations and product distributions therefore predicted.

To reduce the simulation time, the transition structures **B** and **D** were chosen as starting points for the trajectories since these are the reaction path bottlenecks. Initial conditions were determined by random sampling of each excited-state normal mode within an energy threshold $\Delta E_{\text{limit}}$ per mode, leading to a displaced geometry in the vicinity of the transition structure. The trajectory was then started from this displaced geometry with no initial momentum. There was no geometry sampling along the transition vector itself: since the surface is not really quadratic, the initial motion from each displaced geometry may include a component along the reaction coordinate. By doing this, we are essentially sampling the "curvature" of the potential energy surface in the region of the transition structure, which may favor motion toward reactants or products. Values of $\Delta E_{\text{limit}}$ between $0.0005E_h$ and $0.007E_h$ were used, and at least 128 trajectories were run for each. Figure 1 shows that, as $\Delta E_{\text{limit}}$ is increased for path **ADE**, both the initial "spread" and the mean energy of this distribution increases. A total of 768 trajectories starting at displaced geometries up to ~38 kcal mol$^{-1}$ above the transition structure were run. One could contemplate trajectories at higher energies, but there is then a danger of generating geometries that lie outside the region of validity of the MMVB potential (e.g. those with very large C−C $\sigma$-bond distances).

It could be argued that it would be more realistic to simulate the photoexcitation process itself rather than sampling the excited state surface. However, for this system it is not really possible, because we do not know what the optically excited state is. Further, MMVB is limited to covalent states and the optically excited state may be zwitterionic. Thus we make the tacit assumption that decay from any higher energy optically excited state is rapid and that the product yields are mainly controlled

(14) (a) Forbes, W. F.; Shilton, R.; Balasubramanian, A. *J. Org. Chem.* **1964**, *29*, 3527−3531. Ratio of trans:cis butadiene at RTP = 96:4. (b) Smith, W. B.; Massingill, J. L. *J. Am. Chem. Soc.* **1961**, *83*, 4301−4302.

(15) Liu, R. S. H.; Turro, N. J.; Hammond, G. S. *J. Am. Chem. Soc.* **1965**, *87*, 3406−3412.

(16) (a) Bernardi, F.; Olivucci, M.; Robb, M. A. *J. Am. Chem. Soc.* **1992**, *114*, 1606−1616. (b) Bearpark, M. J.; Bernardi, F.; Olivucci, M.; Robb, M. A.; *Chem. Phys. Lett.* **1994**, *217*, 513−519.

(17) Allinger, N. L. *Adv. Phys. Org. Chem.* **1976**, *13*, 1

(18) (a) Anderson, P. W. *Phys. Rev.* **1959**, 115, 2. (b) Said, M.; Maynau, D.; Malrieu, J.-P.; Bach, M.-A. G. *J. Am. Chem. Soc.* **1984**, *106*, 571−579. (c) Said, M.; Maynau, D.; Malrieu, J.-P. *J. Am. Chem. Soc.* **1984**, *106*, 580−587(d) Durand, P.; Malrieu, J.-P. *Adv. Chem. Phys.* **1987**, *67*, 321−412.

(19) (a) Bearpark, M. J.; Bernardi, F.; Clifford, S.; Olivucci, M.; Robb, M. A.; Vreven, T. *J. Phys. Chem. A*, **1997**, *101*, 3841−3847. (b) Bearpark, M. J.; Bernardi, F.; Olivucci, M.; Robb, M. A. *J. Phys. Chem. A*, **1997**, *101*, 8395−8401.

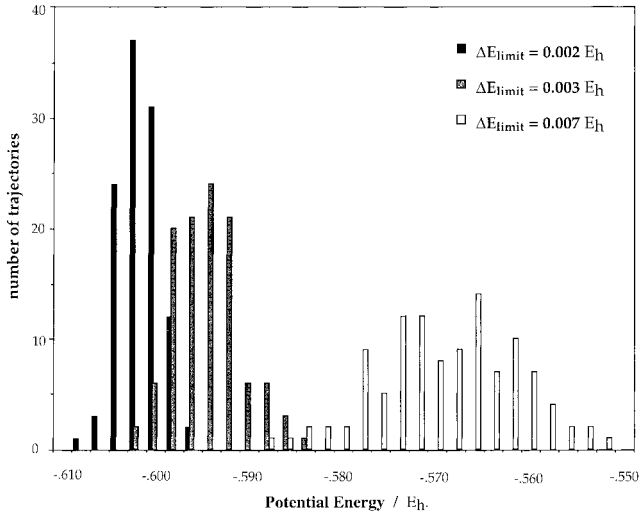


**Figure 1.** Initial potential energy distributions for MMVB trajectories along **ADE** with $\Delta E_{\text{limit}} = 0.002E_h$, $0.003E_h$, and $0.007E_h$. ($\Delta E_{\text{limit}}$ is the limit to energy changes caused by initial random displacements along each excited-state normal mode).

by the transition state bottlenecks that occur on the covalent $S_1$ state.

For each reaction path (**ABC** and **ADE**, Scheme 1) classical trajectories were propagated on the MMVB potential energy surface, as described in ref 2. The method avoids the explicit calculation of the total surface by constructing a sequence of local quadratic approximations[20,21] to the true surface along the classical trajectory. Thus the local surfaces (i.e. gradient and Hessian) are calculated "on the fly" as required during the course of the integration and only those parts of the surface actually traversed by the molecule are therefore considered. The stepsize is determined by a trust radius; the value used was 0.108 $\sqrt{}$amu·bohr, which corresponds to a typical time step of 0.3 fs.

The surface hop algorithm of Tully and Preston[22] was used to allow excited-state trajectories to transfer to the ground state at points in the conical intersection region[23] where nonadiabatic coupling is strong. At each point on the excited-state surface the "hop probability" is determined. When this oscillatory hop probability function has a maximum close to 1, the trajectory is continued on the ground state. The excess energy corresponding to the "gap" is then added to the momentum along the direction of the nonadiabatic derivative coupling vector to conserve the total energy.

At the conical intersection, there are two linearly independent nuclear coordinates—the nonadiabatic derivative coupling (DCP) and gradient difference (UGD) vectors—which lift the degeneracy.[23d] Although decay can take place at any point on the intersection in principle, the region of the minimum[24] will be favored when excess energy can be dissipated to the surroundings in condensed phases, or when the system has very low excess energy (e.g. cold jet). In these situations, the plane defined by the DCP and UGD vectors will be the one in which initial motion on $S_0$ will take place. At least three different recoupling schemes (in a three or four electron conical intersection) can lead to product valleys and these can be determined using an algorithm we have recently discussed.[13] However, a complete picture of the decay and subsequent rearrangements can only be obtained from a nonadiabatic dynamics simulation, particularly if, as in this case, there are unstable primary photoproducts which undergo rearrangement.

Our central objective in this work is to determine the product yields for various initial conditions. Trajectories were propagated until the product domain was reached or there was a return back to excited reactants. Plots of energy or selected geometric parameters against time were usually sufficient to characterize the product for each trajectory. Where there was any ambiguity, an animation was examined.[25] However, a few $S_0$ trajectories could still not be classified, because the trajectory entered regions of the surface where the MMVB parametrization was invalid.

Finally, we must emphasize that our dynamics simulation cannot emulate real experimental conditions, because no allowance is made for the thermal interaction with the solvent. Thus the product distribution we shall report subsequently does not allow for the fact that some reaction channels may be more heavily "damped" through loss of energy to the solvent.

In previous work[4] the CASSCF potential surface for our model system has been characterized in detail. We conclude this section with a brief discussion of the accuracy of the corresponding MMVB surface. MMVB geometries along the two reaction paths on $S_1$—**ABC** and **ADE** (Scheme 1)—are shown in Figure 2, along with the same points previously located with CASSCF. Relative energies calculated with both methods are also indicated in this figure. The minimum energy path (MEP) has been computed (with MMVB) from the transition structures **B** and **D** in order to characterize the reaction coordinates. The MEP is a trajectory with its momentum set to zero at each step and is a lower energy bound for any other trajectory. For both paths **ABC** and **ADE**, the reverse MEP terminates at the $S_1$ minimum **A**, and in the forward direction (Figures3 and 4) it leads to the conical intersection region. In path **ABC** (Figure 3), the reaction coordinate is dominated by the torsion, which brings together one ethylene group from each butadiene. In path **ADE** (Figure 4), the reaction coordinate mainly involves the formation of a new $\sigma$-bond. In addition, the MEPs show that **C** and **E** are "peaked" conical intersections according to the classification of Ruedenberg et al.:[23d] both crossings are energy minima on $S_1$, where the gradient does not go to zero.

The MMVB-optimized geometries (Figure 2) are qualitatively the same as the CASSCF-optimized ones,[4] but

(20) (a) Helgaker, T.; Uggerud, E.; Jensen, H. J. *Chem. Phys. Lett.* **1990**, *173*, 145. (b) Helgaker, T. *J. Phys. Chem.* **1991**, *95*, 4618.

(21) Chen, W.; Hase, W. L.; Schlegel, H. B. *Chem. Phys. Lett.* **1994**, *228*, 435.

(22) Tully, J. C.; Preston, R. K. *J. Chem. Phys.* **1971**, *55*, 562−572.

(23) A conical intersection is an $(n-2)$ dimensional subspace of $(n)$ nuclear coordinates in which two states are degenerate. Movement along the two remaining linearly independent nuclear coordinates (the nonadiabatic coupling and gradient difference vectors) lifts the degeneracy. (a) Herzberg, G. *The Electronic Spectra of Polyatomic Molecules*; Van Nostrand: Princeton, 1966; p 442. (b) Teller, E. *Israel J. Chem.* **1969**, *7*, 227−235. (c) Bonacic-Koutecky, V.; Koutecky, J.; Michl, J. *Angew. Chem., Int. Ed. Engl.* **1987**, *26*, 170−189. (d) Atchity, G. J.; Xantheas, S. S.; Ruedenberg, K. *J. Chem. Phys.* **1991**, *95*, 1862−1876. (e) Manthe, U.; Köppel, H. *J. Chem. Phys.* **1990**, *93*, 1658−1669. (f) Bernardi, F.; Olivucci, M.; Robb, M. *Isr. J. Chem.* **1993**, *33*, 265.

(24) (a) Ragazos, I. N.; Robb, M. A.; Bernardi, F.; Olivucci, M. *Chem. Phys. Lett.* **1992**, 197, 217−223. (b) Bearpark, M. J.; Robb, M. A.; Schlegel, H. B. *Chem. Phys. Lett.* **1994**, 223, 269−274.

(25) Using Moviemol 1.1: Hermansson, K.; Ojamäe, L. Uppsala University, Institute of Chemistry, Report UUIC-B19-500, 1994

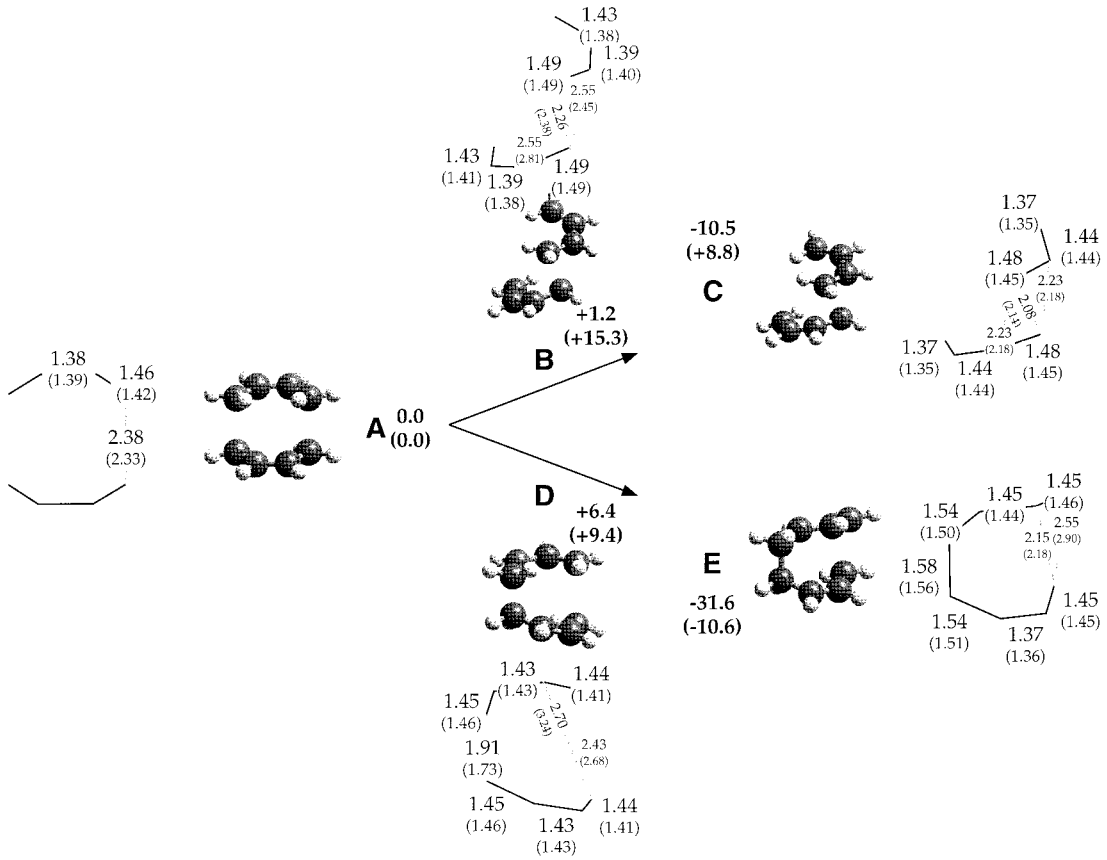


**Figure 2.** The $S_1$ potential energy surface topology predicted by MMVB. Optimized bond lengths/Å are shown for the pericyclic minimum **A**, transition structures **B** and **D**, and $S_0/S_1$ conical intersections **C** and **E**. Relative energies/kcal mol$^{-1}$ (bold face) are also indicated. (CASSCF values for bond lengths and energies, in parentheses, are taken from ref 4).

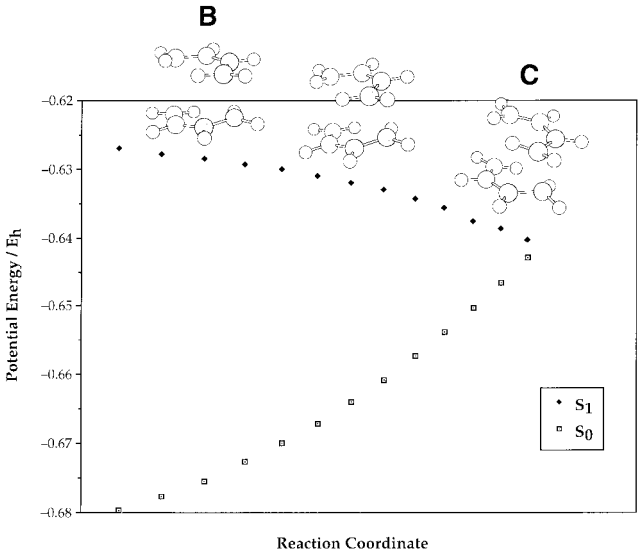


**Figure 3.** Minimum energy path (MEP) computed from the transition structure **B** for the **ABC** path defined in Scheme 1.

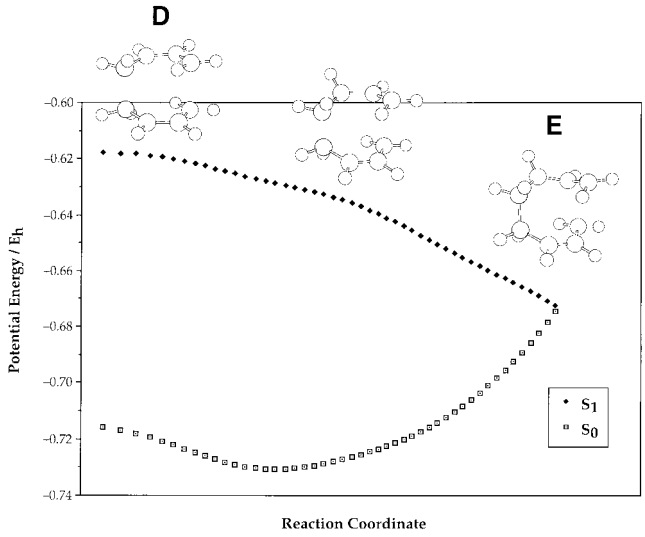


**Figure 4.** Minimum energy path (MEP) computed from the transition structure **D** for the **ADE** path defined in Scheme 1.

there are some differences in detail. At **C**, for example, the length of well-defined double bonds calculated with CASSCF (1.35 Å) is underestimated (1.37 Å) by MMVB. Consequently, there are differences in the energetics: MMVB correctly predicts **E** to be the lowest energy point on $S_1$ overall, but the energy of both **C** and **E** below **A** is overestimated by ~20 kcal mol$^{-1}$ compared with CASSCF. Furthermore, MMVB predicts the barrier height at **D** to be higher than that at **B**, the reverse of the CASSCF prediction. For each trajectory, MMVB will therefore exaggerate the amount of kinetic energy available at the crossing point, which may affect the calculated product distributions.

Both conical intersections **C** and **E** are tetraradicaloids (Scheme 1). The intersection **C** has two pairs of delocalized electrons centered in two ethylene-like fragments and resembles the rhomboidal funnel for the [2 + 2] addition of ethylene + ethylene.[26a,b,d,27] In contrast, the intersection **E** has three electrons delocalized in a propyl-

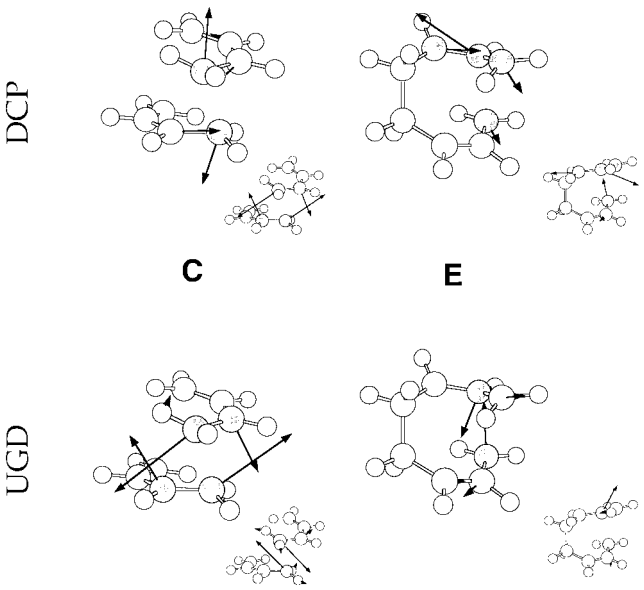


**Figure 5.** The derivative coupling (DCP) and gradient difference (UGD) vectors—those which lift the degeneracy—computed with MMVB at the conical intersections **C** and **E**. The corresponding CASSCF vectors (taken from ref 4) are shown inset.

like fragment (labeled 1−2−3 in *S*cheme 1), and a fourth localized electron at center 4, similar to the conical intersection characterized for methyl migration in but-1-ene.[26c] In Figure 5, the UGD and DCP belonging to conical intersection minima **C** and **E** are compared to those obtained at the CASSCF/4-31G level.[4] An animation of the UGD and DCP vectors shows that CASSCF and MMVB predict the same initial motions, although from Figure 5 we can see that these vectors are swapped for **C**. This swap is not important since the branching space[23d] is defined by the plane of the two vectors and thus remains unchanged.

### 3. Results and Discussion

In this section we will discuss the results of surface hopping dynamics simulations for the two independent excited-state reaction channels **ABC** and **ADE** (Scheme 1). The yields of the photoproducts originating from each channel will be determined by assigning each trajectory starting at the transition structure to a particular ground-state product ($\mathbf{P_{b-g}}$, Scheme 2; $\mathbf{P_b}$ is $S_0$ butadiene + butadiene, which is a "product" in this simulation) or to the excited-state reactant (**A**). In this way we can estimate the product distribution for the corresponding channel.

We assume that the branching between paths **ABC** and **ADE** is controlled by the barriers at **B** and **D**, respectively. Entropy may be an important factor in the branching between the two paths. We have explored this point by comparing the number of excited-state trajectories which reach the conical intersection with the number which return to the excited-state reactants.

**Table 1. MMVB Dynamics: Computed Yields of $\mathbf{P_c}$ ($S_0$ 1,3-divinylcyclobutane), $\mathbf{P_b}$ ($S_0$ butadienes), and A ($S_1$ Pericyclic Minimum) as a Function of the Energy Sampling Parameter $\Delta E_{\mathrm{Limit}}$ in Vibrational Modes Orthogonal to the Reaction Path ABC (Figure 2)[a]**

| $\Delta E_{\mathrm{limit}}/E_h$ | % hopped to $S_0$ | % $\mathbf{P_c}$ | % $\mathbf{P_b}$ | % other $S_0$ product[c] | % **A**[b] |
|---|---|---|---|---|---|
| 0.0005 | 49.2 | 37.5 | 4.7 | 7.0 | 50.8 |
| 0.001 | 53.7 | 41.9 | 4.4 | 7.4 | 46.3 |
| 0.002 | 42.2 | 27.1 | 4.2 | 11.0 | 57.8 |
| 0.003 | 39.8 | 25.0 | 6.3 | 8.6 | 60.2 |
| 0.005 | 32.8 | 21.1 | 5.5 | 6.3 | 67.2 |
| 0.007 | 35.2 | 18.0 | 7.8 | 9.4 | 64.8 |

[a] **A**, $\mathbf{P_b}$, and $\mathbf{P_c}$ are illustrated in Scheme 2. [b] Remains on $S_1$. [c] Structure could not be determined.

**Table 2. MMVB Dynamics: Surface Hop Data for the ABC (Figure 2) Trajectories Leading to Product $\mathbf{P_c}$ (Scheme 2) as a Function of the Energy Sampling Parameter $\Delta E_{\mathrm{limit}}$**

| $\Delta E_{\mathrm{limit}}/E_h$ | initial $S_1$ energy[a]/ kcal mol$^{-1}$ | $S_1$ hop energy[a]/ kcal mol$^{-1}$ | $\Delta E$ at hop/ kcal mol$^{-1}$ | KE at hop/ $\times 10^{-2}$ $E_h$ | time to hop/fs |
|---|---|---|---|---|---|
| 0.0005 | 2.6 ± 0.3 | −6.3 ± 0.6 | 2.2 ± 1.0 | 1.4 ± 0.1 | 123 ± 35 |
| 0.001 | 5.1 ± 0.7 | −4.9 ± 0.8 | 2.4 ± 1.0 | 1.6 ± 0.1 | 115 ± 31 |
| 0.002 | 9.5 ± 1.5 | −2.7 ± 1.6 | 2.6 ± 1.1 | 2.0 ± 0.2 | 104 ± 26 |
| 0.003 | 14.0 ± 2.0 | 0.0 ± 1.8 | 2.6 ± 1.3 | 2.3 ± 0.3 | 107 ± 34 |
| 0.005 | 22.3 ± 2.7 | 4.1 ± 1.9 | 3.5 ± 1.1 | 2.9 ± 0.4 | 94 ± 27 |
| 0.007 | 29.3 ± 3.7 | 7.7 ± 3.2 | 3.7 ± 1.5 | 3.4 ± 0.4 | 86 ± 25 |

[a] Energy relative to the transition structure **B**.

**Reaction Path ABC.** The three primary $S_0$ products for path **ABC** are indicated in Scheme 1, corresponding to the feasible ways of recoupling the four uncoupled electrons indicated at **C**. The product yields for our **ABC** simulation are given in Table 1. (Note that the column "% other $S_0$ product" refers to trajectories that went to regions where the MMVB potential was invalid. Thus the dispersion in the product yields must reflect this effect in part). Values for the sampling parameter $\Delta E_{\mathrm{limit}}$ of between $0.0005E_h$ and $0.007E_h$ were used, corresponding to initial excess energies (energies of the displaced starting geometries above **B**) of ∼3 to ∼30 kcal mol$^{-1}$. Since our trajectories start in the vicinity of the transition structure **B**, we might expect 50% to go to the pericyclic minimum **A** and the other 50% to go to the intersection **C**. However, Table 1 shows that this is not the case: increasing $\Delta E_{\mathrm{limit}}$ reduces the number of trajectories which reach the conical intersection region ("% hopped to $S_0$" in Table 1), implying that the valley connecting the TS to the conical intersection is "narrower" than the valley connecting the TS to the pericyclic minimum. We therefore expect a rather high activation entropy for this process. Table 1 also shows that, for those trajectories which decay to $S_0$ in the conical intersection region, the likelihood of return to unreacted butadienes ($\mathbf{P_b}$) increases as more of the crossing region is sampled.

In Table 2, we show all of the data related to the trajectories leading to the $S_0$ [2 + 2] product $\mathbf{P_c}$. For the lowest energy sampling batch ($\Delta E_{\mathrm{limit}} = 0.0005E_h$) with an excess energy of 2.6 ± 0.3 kcal mol$^{-1}$, the trajectories hop to $S_0$ with an average energy of 5 ± 1 kcal mol$^{-1}$ above the $S_1/S_0$ conical intersection minimum **C**. The mean energy gap between both surfaces at the hop is ∼2 kcal mol$^{-1}$ (i.e. the surface hop region is rather small), which indicates that we have a well-defined reaction channel that leads from the transition structure **B** on $S_1$

(26) (a) Bernardi, F.; De, S.; Olivucci, M.; Robb, M. A. *J. Am. Chem. Soc.* **1990**, *112*, 1737−1744. (b) Bernardi, F.; Olivucci, M.; Robb, M. A. *Acc. Chem. Res.* **1990**, *23*, 405−412. (c) Bernardi, F.; Olivucci, M.; Robb, M. A.; Tonachini, G. *J. Am. Chem. Soc.* **1992**, *114*, 5805−5812. (d) Celani, P.; Bernardi, F.; Olivucci, M.; Robb, M. A. *J. Chem. Phys.* **1995**, 102, 5733−5742.

(27) (a) Michl, J. *Pure App. Chem.* **1975**, *41*, 507−534. (b) Gerhartz, W.; Poshusta, R. D.; Michl, J.; *J. Am. Chem. Soc.* **1976**, *98*, 6427−6443. (c) Gerhartz, W.; Poshusta, R. D.; Michl, J. *J. Am. Chem. Soc.* **1977**, *99*, 4263−4271.

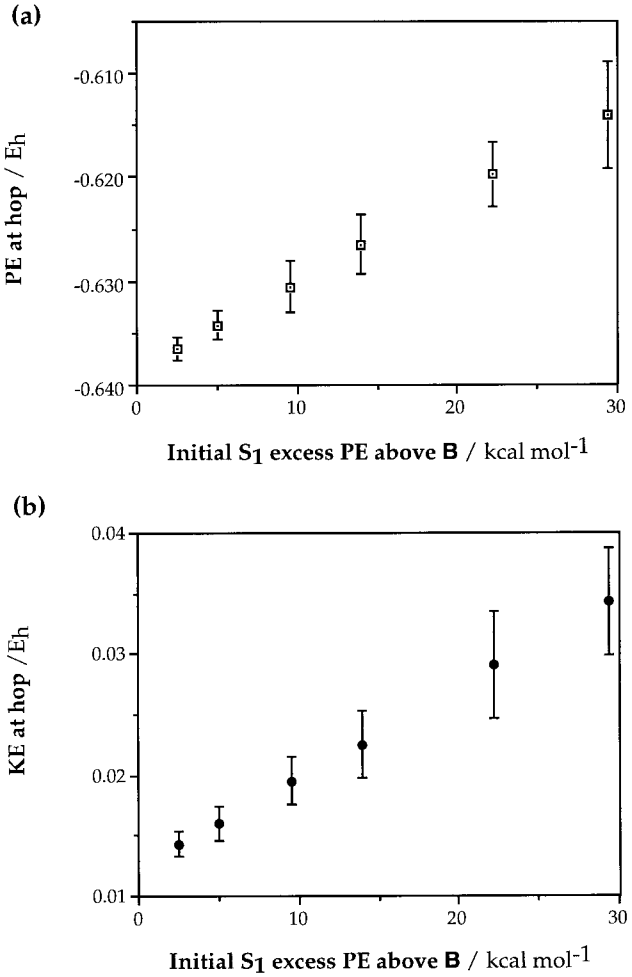


**Figure 6.** (a) The distribution of potential energies for all trajectories hopping at the $S_0/S_1$ intersection **C**. (b) The distribution of kinetic energies at the $S_1 \rightarrow S_0$ hop. (Data from Table 2.)

to **C**. The hop need not occur at the minimum in the crossing region, since, in our system, the conical intersection hyperline is 52-dimensional. In fact, it is very unlikely that any trajectory could encounter the lowest energy point. This result is also shown by Figure 6a: the $S_1$ potential energy at which the hop occurs increases as the potential energy of the initial $S_1$ geometry above **B** increases. The standard deviation of the hop energies increases because the initial potential energy distribution has a wider spread and hence trajectories can access higher energy points on the conical intersection hyperline. Figure 6b shows the same trend in the transformation of initial energy sampling ($\Delta E_{limit}$) into kinetic energy at the intersection.

**Reaction Path ADE**. The analysis of the trajectories excited at TS **D**, which hop to $S_0$ (Table 3), shows that three main channels are populated; none of these correspond to a return to the $S_0$ reactant minimum $\mathbf{P_b}$. These channels lead to (i) a [4 + 4] primary product, 1,5-cyclooctadiene, $\mathbf{P_g}$; (ii) a [2 + 2] secondary product, 1,2-divinylcyclobutane, $\mathbf{P_d}$; and (iii) two possible [2 + 4] products, 4-vinyl-1-cyclohexene, $\mathbf{P_e}$ (primary), and 4-vinylbicyclo[1.0.3]hexane, $\mathbf{P_f}$ (secondary).

In contrast with path **ABC**, a large percentage (~90%) of **ADE** trajectories reach the conical intersection **E**, as shown in Table 3. This is mainly due to the fact that **E** is an intramolecular intersection while **C** is an intermolecular intersection and can easily fragment back (i.e. there is no $\sigma$-bond keeping the pieces together). Most of the trajectories that hop end up at $\mathbf{P_e}$ and $\mathbf{P_f}$, which are the major experimental products.[5] Table 3 also shows that the amount of geometry sampling hardly affects the computed quantum yields of the photoproducts, in contrast to path **ABC**. The reason for this is related to the energetics of both reaction pathways. While in path **ABC** the energy difference (exothermic) between the transition structure and the minimum of the conical intersection is ~12 kcal mol$^{-1}$ (Figure 2), the corresponding difference in path **ADE** is calculated to be ~38 kcal mol$^{-1}$. Thus the steeper initial gradient reduces the effect of initial conditions for **ADE** due to a large acceleration along the reaction coordinate.

**Table 3. MMVB Dynamics: Computed Yields of $\mathbf{P_e}$ ($S_0$ 4-vinyl-1-cyclohexene) and $\mathbf{P_f}$ ($S_0$ 4-vinylbicyclo[1.0.3]hexane), $\mathbf{P_g}$ ($S_0$ 1,5-cyclooctadiene), $\mathbf{P_d}$ ($S_0$ 1,2-divinylcyclobutane), and A ($S_1$ Pericyclic Minimum) as a Function of the Energy Sampling Parameter $\Delta E_{Limit}$ in Vibrational Modes Orthogonal to the Reaction Path ADE (Figure 2)[a]**

| $\Delta E_{limit}/E_h$ | % hopped to $S_0$ | % $\mathbf{P_e}$ & $\mathbf{P_f}$ | % $\mathbf{P_g}$ | % $\mathbf{P_d}$ | % other $S_0$ product[c] | % **A**[b] |
|---|---|---|---|---|---|---|
| 0.0005 | 89.8 | 39.8 | 14.8 | 12.5 | 22.7 | 10.2 |
| 0.001 | 92.0 | 38.7 | 23.1 | 9.0 | 21.1 | 8.0 |
| 0.002 | 93.8 | 48.4 | 14.8 | 7.8 | 22.7 | 6.3 |
| 0.003 | 89.8 | 43.8 | 13.3 | 14.1 | 18.8 | 10.2 |
| 0.005 | 85.9 | 41.4 | 15.6 | 8.6 | 20.3 | 14.1 |
| 0.007 | 85.9 | 43.0 | 14.1 | 2.3 | 26.6 | 14.1 |

[a] **A**, $\mathbf{P_{d-g}}$ are illustrated in Scheme 2. [b] Remains on $S_1$. [c] Structure could not be determined.

**Table 4. MMVB Dynamics: Surface-Hop Data for the ADE (Figure 1) Trajectories Leading to $S_0$ Products $\mathbf{P_e}$ and $\mathbf{P_f}$, $\mathbf{P_g}$, and $\mathbf{P_d}$ as a Function of the Energy Sampling Parameter $\Delta E_{limit}$[a]**

| $\Delta E_{limit}/E_h$ | initial $S_1$ energy[b]/ kcal mol$^{-1}$ | $S_1$ hop energy[a]/ kcal mol$^{-1}$ | $\Delta E$ at hop/ kcal mol$^{-1}$ | KE at hop/ $\times 10^{-2}$ $E_h$ | time/fs |
|---|---|---|---|---|---|
| | | $\mathbf{P_e}$ & $\mathbf{P_f}$ | | | |
| 0.0005 | 2.6 ± 0.4 | −14.5 ± 4.5 | 5.2 ± 1.5 | 4.9 ± 0.4 | 73 ± 18 |
| 0.001 | 5.4 ± 0.8 | −14.1 ± 5.4 | 5.2 ± 1.5 | 5.0 ± 0.6 | 71 ± 19 |
| 0.002 | 9.9 ± 1.4 | −11.6 ± 6.2 | 4.6 ± 1.7 | 5.4 ± 0.6 | 71 ± 19 |
| 0.003 | 14.2 ± 2.0 | −8.8 ± 5.8 | 4.8 ± 1.5 | 5.6 ± 0.8 | 75 ± 18 |
| 0.005 | 22.8 ± 3.5 | −5.3 ± 6.0 | 5.0 ± 1.7 | 6.5 ± 0.7 | 65 ± 18 |
| 0.007 | 28.9 ± 4.5 | −0.1 ± 8.4 | 4.3 ± 8.6 | 6.6 ± 0.9 | 65 ± 16 |
| | | $\mathbf{P_g}$ | | | |
| 0.0005 | 2.6 ± 0.4 | −17.8 ± 4.6 | 3.2 ± 1.3 | 5.1 ± 0.6 | 72 ± 10 |
| 0.001 | 5.1 ± 0.8 | −15.5 ± 4.4 | 3.5 ± 1.6 | 5.2 ± 0.6 | 72 ± 14 |
| 0.002 | 9.7 ± 1.2 | −14.5 ± 4.1 | 3.0 ± 1.6 | 5.6 ± 0.6 | 63 ± 6 |
| 0.003 | 13.9 ± 2.5 | −8.5 ± 5.5 | 3.5 ± 1.4 | 5.4 ± 0.8 | 72 ± 16 |
| 0.005 | 22.1 ± 3.4 | −6.7 ± 5.3 | 3.3 ± 1.4 | 6.3 ± 0.6 | 69 ± 15 |
| 0.007 | 29.5 ± 3.5 | 0.7 ± 6.5 | 3.8 ± 1.2 | 6.4 ± 1.0 | 75 ± 12 |
| | | $\mathbf{P_d}$ | | | |
| 0.0005 | 2.6 ± 0.5 | −17.1 ± 3.6 | 3.5 ± 1.3 | 4.9 ± 0.5 | 80 ± 13 |
| 0.001 | 5.4 ± 0.5 | −12.7 ± 6.0 | 3.5 ± 0.9 | 4.7 ± 0.7 | 79 ± 15 |
| 0.002 | 9.4 ± 1.4 | −13.4 ± 5.7 | 3.9 ± 1.2 | 5.4 ± 0.7 | 74 ± 11 |
| 0.003 | 14.3 ± 2.7 | −6.8 ± 7.9 | 3.9 ± 1.5 | 5.3 ± 1.0 | 72 ± 12 |
| 0.005 | 22.4 ± 3.0 | −6.2 ± 3.8 | 3.6 ± 1.8 | 6.6 ± 0.5 | 66 ± 14 |
| 0.007 | 33.5 ± 1.9 | 1.6 ± 3.5 | 3.7 ± 1.0 | 7.1 ± 0.6 | 92 ± 8 |

[a] $\mathbf{P_{d-g}}$ are illustrated in Scheme 2. [b] Energy relative to the transition structure **D**.

Table 4 shows all the data related to the hop leading to the **ADE** [2 + 4], [4 + 4], and [2 + 2] products. Notice that the surface hops in the lowest energy sampling batch ($\Delta E_{limit} = 0.0005 E_h$) occur around 20 kcal mol$^{-1}$ above the $S_1/S_0$ conical intersection minimum **E**, irrespective of the photoproduct reached. This fact can be interpreted in terms of the curvature of the $S_1$ reaction path leading to the conical intersection hyperline: if the reaction path

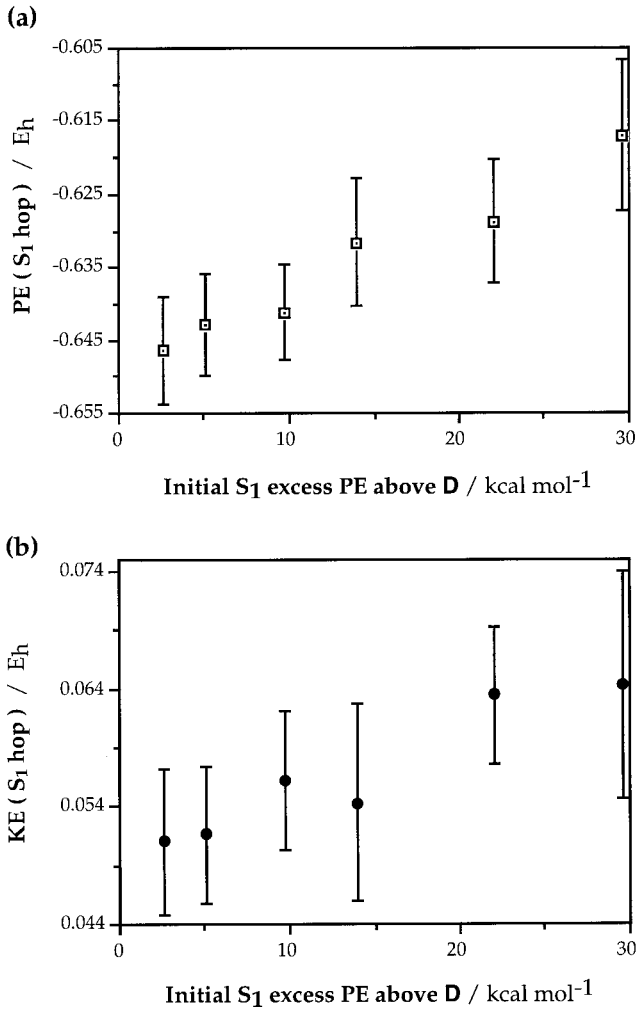


**Figure 7.** (a) The distribution of potential energies for all trajectories hopping at the $S_0/S_1$ intersection **E**. (b) The distribution of kinetic energies at the $S_1 \rightarrow S_0$ hop. (Data from Table 4.)

leading **D** to **E** is curved, the system will develop vibrations orthogonal to the reaction path as the direction changes, and surface hops can occur at higher energy points on the hyperline. This is also seen when we plot the hop energies (Figure 7): although the mean energy increases (as for path **ABC**, Figure 6), the standard deviation for **ADE** is approximately constant. The effects of the initial geometry sampling are lost due to vibrations generated in the reaction channel itself.

## 4. Conclusion

MMVB dynamics has been used to model the product distribution for the [4 + 4] photocycloaddition of butadiene + butadiene. (The MMVB geometries and energetics of all the critical points involved in both paths on $S_1$ are supported by previous CASSCF calculations[4]). Photoproduct formation begins at two different conical intersections where the $S_1 \rightarrow S_0$ decay can be fully efficient. These two conical intersections can be related to crossings already characterized in conjugated hydrocarbons. From each crossing, a mixture of products can be generated.

The existence of two independent crossings and unstable primary photoproducts suggests that product yield will be a complex function of experimental conditions. However, the major experimental product has been correctly predicted by means of MMVB dynamics. These results can be related to other systems such as cyclohexadiene + naphthalene,[9] where the restricted rotation will favor some products but not others, and anthracene + anthracene,[10c,d] where the bonding in the 9−10-position can be established and one product stabilized exclusively.

**Acknowledgment.** This research has been supported in part by the EPSRC (UK) under grants GR/J25123 and GR/H58070. MMVB dynamics calculations were run on a Cray T3D at the Parallel Computing Centre, University of Edinburgh (EPCC). Some images were created with MacMolecule, University of Arizona.

JO972111V